Hindawi
Geofluids
Volume 2022, Article ID 2405177, 13 pages
https://doi.org/10.1155/2022/2405177

Research Article

Seismic Damage Analysis of Large-Span Tied-Arch Bridge with Concrete-Filled Steel Tubes Subjected to Near-Fault Ground Motion

Yingzhi Xia, Jiawei Liu, Hui Li, and Guoping Hu

School of Civil and Transportation Engineering, Henan University of Urban Construction, Longxiang Road, Xincheng Area, Pingdingshan, Henan 467036, China

Correspondence should be addressed to Jiawei Liu; liujiawei@hncj.edu.cn

Received 19 April 2022; Revised 15 September 2022; Accepted 19 September 2022; Published 11 October 2022

Academic Editor: Di Feng

In this study, the damage mechanism due to near-fault ground motions on large-span arch bridges with concrete-filled steel tubes was investigated based on a case study. A tied-arch bridge with concrete-filled steel tubes with a span of 460 m has been examined using the numerical simulation method. The performance of the bridge was analyzed in terms of displacement, overall response, internal force changes, and damage probability considering the various near-fault and non-near-fault ground motions when imposing load onto the bridge. Then, the relationship between the bridge damage and the design parameters of ground motion intensities, near-fault velocity pulse, and excitation angle was obtained. The results indicated that the probability of damage caused by near-fault earthquakes is significantly higher than that by non-near-fault ground motions, and velocity pulses may cause more severe damages to certain components of the bridge during lower-intensity ground motions at certain excitation angles. And the damage furtherly resulted in the weakening of the bridge structure and decrease in its load-carrying capacity. Therefore, the near-fault ground motion should be fully considered in the design of large-span arch bridges with concrete-filled steel tubes in practical engineering.

1. Introduction

Concrete-filled steel tubes have good mechanical properties by optimizing the material properties of both steel and concrete [1]. And they have been widely used in recent decades, especially in arch bridges [2, 3]. In China, more than 400 arch bridges use concrete-filled steel tubes to prevent buckling of the arch. Arch bridges that use concrete-filled steel tubes have been constructed with a maximum span of 575 m [4, 5]. Arch bridges are economical, practical, and ideal for crossing places that cannot be accessed and difficult to build midspan supports, such as rivers, mountain valleys, deep gorges, and where large pier foundations are required [6, 7]. The arch support on both sides of the valley can be anchored into the bedrock when concrete-filled steel tubes are used. There are mainly three different types of modern arch bridges for roadway transportation: deck arch, through arch, and tied arch bridges [8, 9]. In Southwest China, there is a rapid increase to altitudes with numerous valleys and a large number of rivers between the Qinghai-Tibet Plateau (also known as the Tibetan Plateau) and Sichuan Basin, which shows a high demand for bridges in this region [10]. The arch bridges with concrete-filled steel tubes are ideal in the mountainous terrain; the challenges facing the construction of arch bridges result in a "bottleneck" on road network development, which directly affects the capacity of the roadways and the efficiency of the transportation systems [5, 11, 12]. Moreover, Southwest China is one of the most seismically active areas. In recent decades, there have been various earthquakes with large scale, such as the Wenchuan or Sichuan earthquake in 2008 with a magnitude of 8 on the Richter scale, the Lushan or Ya'an earthquake in 2013 with a magnitude of 7, the Yushu earthquake in 2010 with a magnitude of 6.9, and the Jiuzhaigou earthquake in 2017 with a magnitude of 7. If the highways become damaged during an earthquake, emergency access to the affected area for rescue

Table 1: List of near-fault earthquakes with pulse-like ground motions.

Sequence number	Earthquake name	Station name	Magnitude	Closest distance (km)	Tp (s)	PGV (cm/s)	Orientation (°)
1	Taiwan SMART1(40)	C00	6.3	59.9	1.57	34.8	117
2	Taiwan SMART1(40)	E01	6.3	57.3	1.39	36.9	104
3	Taiwan SMART1(40)	I01	6.3	60.1	1.57	32.9	113
4	Taiwan SMART1(40)	I07	6.3	59.7	1.67	34.0	113
5	Taiwan SMART1(40)	M01	6.3	60.9	1.39	26.1	111
6	Taiwan SMART1(40)	M07	6.3	58.9	1.54	40.4	114
7	Taiwan SMART1(40)	O07	6.3	58.0	1.53	28.7	106
8	Kobe, Japan	KJMA	6.9	1.0	1.09	105.6	318
9	Parkfield-02, CA	EADES	6.0	2.9	1.22	35.8	41
10	Parkfield-02, CA	Slack canyon	6.0	3.0	0.85	53.2	0
11	Parkfield-02, CA	Cholame 1E	6.0	3.0	1.33	51.6	58
12	Joshua Tree, CA	Jackson Road	6.1	25.5	1.10	53.3	268
13	Darfield, New Zealand	CBGS	7.0	18.1	12.62	59.9	346
14	Darfield, New Zealand	DSLC	7.0	8.5	7.83	65.9	44
15	Christchurch, New Zealand	CCCC	6.1	3.3	1.72	66.9	266
16	Christchurch, New Zealand	CHHC	6.1	4.8	1.96	81.3	57
17	Christchurch, New Zealand	CMHS	6.1	4.5	2.04	48.1	21
18	Christchurch, New Zealand	HPSC	6.1	4.3	6.85	48.3	291
19	Christchurch, New Zealand	PRPC	6.1	2.0	4.82	123.1	135
20	Christchurch, New Zealand	REHS	6.1	5.1	1.55	97.5	71

Notes: orientation refers to that of the strongest pulse, in degrees clockwise from the north, and PGV is the peak ground velocity.

and disaster relief will be seriously affected [13, 14], which verified the extreme importance of the integrity of the highways. Therefore, seismic performance is one of the critical design parameters that must be considered in the construction of highway bridges [15, 16]. In theory, bridges should not be built near large active faults that are hundreds to thousands of metres in depth. However, there are a number of reasons why crossing these faults cannot be avoided in reality [17, 18]. For instance, the area on the highway route has a dense network of faults and the construction costs of rerouting could be higher. And there might be topographic limitations and an overall lack of other options aside from building bridges. Bridges crossing a fault will very likely suffer serious near-fault ground motions due to an earthquake during the design lifetime [19–21].

However, near-fault ground motions carry high-energy pulses with a frequency that can approach the fundamental natural frequency of large-span bridge structures, which easily transfer a large amount of seismic energy onto the bridge structure and cause serious damage [22, 23]. Ensuring the safety of large-span arch bridges during near-fault ground motions has become an important issue, especially for bridges with concrete-filled steel tubes, to prevent the "bottleneck effect" on the road networks [24, 25]. A large volume of studies has been done on this topic. Near-fault ground motions have an important characteristic—the occurrence of large velocity pulses which originate from the effects of directivity during an earthquake [26, 27]. The effects of near-fault velocity pulses on concrete-filled steel tube arch bridges with reinforced concrete arched ribs on either side of the span have been examined [28, 29]. As for the earthquake resistance of bridges and other structures, the transmission process of seismic load and the input mode of load are closely related to the characteristics of foundation soil. The mechanical characteristics of soil, the influence of constitutive model, and the input characteristics of ground motion are very important to the safety of bridge structures [30, 31].

The connection between the arch ribs and the bridge deck is the most vulnerable area on the bridge. Li et al. [32] used a spectrum compatible method to select the most common naturally occurring near-fault ground motions based on site records from the Pacific Earthquake Engineering Research Center (PEER) database of the University of California, USA. The effect of velocity pulses on the seismic response of actual arch bridges with concrete-filled steel tubes were examined. The results showed that the velocity pulse, pulse duration, the multidirectional movement of the earthquake, and the conditions on which the bridge is constructed all have a significant effect on the seismic response of the bridge structure [33]. Liu et al. [34, 35] used a bridge vulnerability analysis to study the intensity of damage to arch bridges with concrete-filled steel tubes caused by near-fault ground motions. Miyamoto et al. [36] used the Saikai Bridge in Japan as a case study and made actual measurements to calibrate the vibration modeling to obtain more accurate seismic responses.

These studies all demonstrate that near-fault ground motions cause additional damage to large-span arch bridges with concrete-filled steel tubes which are mainly caused by high-velocity pulses. Hence, this study is focused on the damage mechanism of large-span arch bridges with concrete-filled steel tubes due to high-velocity pulses. As a

Table 2: List of non-near-fault earthquakes with pulse-like ground motions.

Sequence number	Earthquake name	Station name	Magnitude	Closest distance (km)	PGA (m/s^2)		PGV (cm/s)	
					Horizontal	Vertical	Horizontal	Vertical
1	TaiwanSMART1(45)	C00	7.3	56.0	1.50	0.71	29.7	6.9
2	TaiwanSMART1(40)	O01	6.3	60.8	1.60	0.21	21.1	3.5
3	TaiwanSMART1(45)	E01	7.3	53.3	1.68	0.66	24.7	5.9
4	TaiwanSMART1(45)	E02	7.3	51.4	1.36	0.41	14.5	4.9
5	TaiwanSMART1(45)	I01	7.3	56.2	1.37	0.74	31.0	7.4
6	TaiwanSMART1(45)	I07	7.3	55.8	1.19	0.82	26.9	7.3
7	TaiwanSMART1(45)	M01	7.3	56.9	1.39	0.80	28.4	5.9
8	TaiwanSMART1(45)	M07	7.3	55.1	1.58	1.04	26.9	9.6
9	TaiwanSMART1(45)	O01	7.3	57.9	1.71	0.49	22.4	6.9
10	Kobe_Japan	Kakogawa	6.9	22.5	3.18	1.68	26.9	9.0
11	Parkfield-02_CA	SanLuisObispo	6.0	61.1	0.10	0.05	1.1	0.4
12	Parkfield-02_CA	CityHallAnnex	6.0	117.9	0.14	0.04	3.2	1.5
13	Parkfield-02_CA	FireStation39	6.0	22.5	0.59	0.23	6.1	3.1
14	Parkfield-02_CA	Hwy58&Wasco	6.0	85.6	0.07	0.03	1.3	0.4
15	Darfield_ NewZealand	CathedralCollege	7.0	19.9	1.81	1.96	59.2	12.6
16	Darfield_ NewZealand	Hospital	7.0	18.4	1.95	1.61	67.2	16.0
17	Darfield_ NewZealand	CashmereHighSchool	7.0	17.6	2.46	2.91	50.4	12.5
18	Darfield_ NewZealand	WAKC	7.0	72.5	1.50	0.63	15.1	7.3
19	Darfield_ NewZealand	WBCS	7.0	207.6	0.21	0.07	3.1	1.9
20	Darfield_ NewZealand	WDFS	7.0	240.8	0.07	0.02	1.0	1.0

Note: PGA denotes peak ground acceleration.

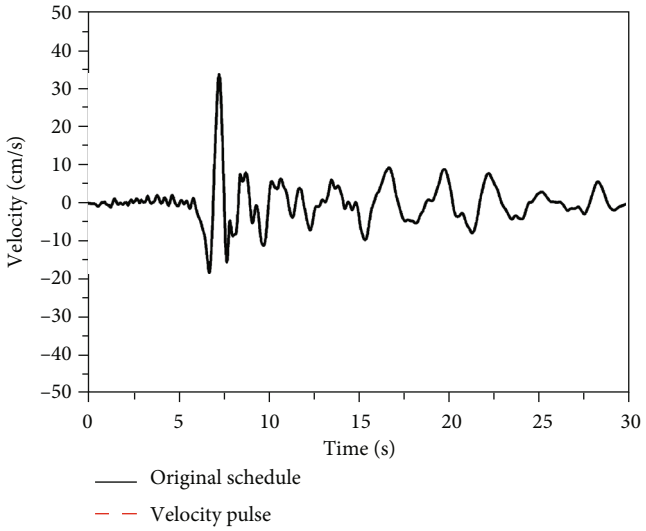

Figure 1: Near-fault velocity pulse extraction results.

case study, a large-span arch bridge with concrete-filled steel tubes and a maximum span of 460 m is analyzed in this study. The bridge is located in Chongqing Province, China, and is called Wushan bridge. It is 19 years old and constructed in 2003. It is a typical example of the large-span tied-arch bridge in China. The near-fault ground motion data from the PEER database for different seismic events are used to calculate the seismic load on the structure. Based on statistical analysis, the impact of the velocity pulse and excitation angle of the ground motion are determined in the key response areas in order to quantitively analyze the overall damage of the bridge.

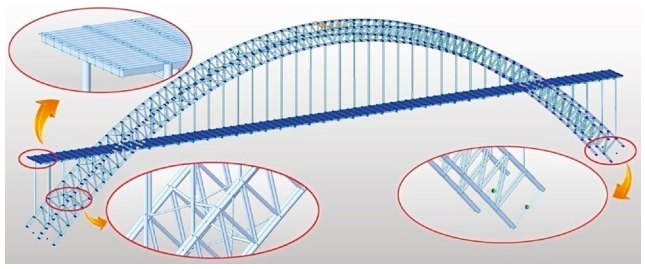

Figure 2: Finite element model of the bridge.

2. Methods and Materials

2.1. Selection of Near-Fault Ground Motions. The high-velocity pulse is one of the most significant characteristics

Table 3: Modal frequencies.

Mode no.	Vibration characteristics	Frequency (Hz)
1	Transverse direction of main arch and bridge deck is symmetrically bent	0.11
2	Transverse direction of main arch and bridge deck is asymmetrically bent	0.18
3	Vertical direction of main arch and bridge is deck asymmetrically bent	0.25
4	Transverse direction of main arch and bridge deck is symmetrically bent in the opposite directions	0.29
5	First order torsion of the main arch and bridge deck	0.34
6	Second order torsion of the main arch and bridge deck	0.53

of near-fault ground motions, which has damaging impacts on nearby permanent structures. Hence, high-velocity pulses are used to identify near-fault ground motions in this study. The wavelet transforms by Shahi and Baker [37] are used to extract the velocity pulses. Wavelet transform allows the transformation only in time, leaving the wave shape unchanged, which shows good representation both in time and temporal frequency and can completely extract pulses and accurately detect the pulse frequency. This method was used to extract 20 representative sets of near-fault ground motions in the PEER database, and 20 sets of the corresponding non-near-fault ground motions as the control cases.

When selecting the near-fault ground motions, the extracted velocity pulse waveforms need to be as rich in detail as possible, with a wide frequency range in order to be used to analyze a variety of conditions and identify the most affected areas on the bridge. Tables 1 and 2 list the records of near-fault and non-near-fault earthquake used in this study, respectively. Figure 1 shows the extracted velocity pulse of No. 1 in Table 1.

The results show that the velocity pulses of all of the near-fault earthquakes have high intensity with concentrated energy, which demonstrate the significant effects of near-fault ground motions. The near-fault earthquakes show longer pulses and higher frequencies which are indicative of the intensity of the ground motions. The corresponding non-near-fault earthquakes with ground motions that have a similar peak acceleration are used for comparison purposes.

2.2. The Finite Element Modeling of the Bridge. This study adopts a tied-arch bridge with concrete-filled steel tubes with a maximum bridge span of 460 m. The main arch is in the shape of a catenary with an arch axis coefficient of 1.55 and a ratio of rise to span of 1/3.8. The bridge deck is 19 m wide. The bridge is supported by a total of 14 K-shaped and 6 criss-cross-shaped cross braces. The 109 steel suspension rods are made of parallel wire strands that are 7 mm in diameter with a tensile strength of 1670 MPa.

The bridge is located in a valley with steep banks on both sides. It is situated on a stratigraphy of hard rock and bare bedrock with high compressive strength. The design load is categorized as Highway I, and there is a Level I waterway under the bridge (based on Chinese standard JTG D60-2015 General Code for Design of Highway Bridges and Culverts) [38], which means that the vehicle load of this large-span bridge is 550 KN. The arch base adopts the combination foundation of enlarged foundation and pile foundation to resist the horizontal thrust. Four piles with a diameter of 300 cm are set at the leading edge of the arch for reinforcement with a depth of 30 m.

The demand for land transportation and shipping is high in this area so this bridge has an extremely important role in the transportation network of this region. A higher seismic resistance level is adopted in design with an intensity of VII on the leidu scale (based on Chinese standard GB/T 17742-2020 China Seismic Intensity Scale) [39].

Based on the design drawings, a large-scale finite element analysis software called Midas is used for the modeling in accordance with the current specifications in China, in which beam element models are used for the upper and lower chords at the arch ribs, webs, wind braces, longitudinal and transverse beams, and arch on the columns. Truss elements are used to simulate the suspension rods, and plate elements are used to simulate the bridge deck. The displacement in the x, y, and z directions was constrained to fix the degrees of freedom in a particular position, and the arch supports are constrained as hinged joints. The high-velocity pulses transfer a large amount of seismic energy onto the structures in a very short period of time, which simulated the process of ground motion transmitted to the bridge structure.

The overall structural model of the bridge is shown in Figure 2, which is based on the subspace iteration method for the modal analysis. The first six modal frequencies of the bridge from the modal analysis are summarized in Table 3.

3. Results and Analysis

Near-fault earthquakes differ from other earthquakes in that high-velocity pulses transfer a large amount of seismic energy onto the structures in a very short period of time. This causes damage to some of the components far greater than the average amount of damage which often leads to complete failure e of the structure. Therefore, this study examines the effects of near-fault earthquakes on a tied-arch bridge from both the local and global aspects of the bridge.

3.1. Analysis of Response of Key Locations. The first set of samples from the group of near-fault earthquakes was used to illustrate the analysis process. The north-south axis was used as the longitudinal excitation direction, the east-west axis as the transverse excitation direction, and the vertical axis as the vertical excitation direction. Midas was also used

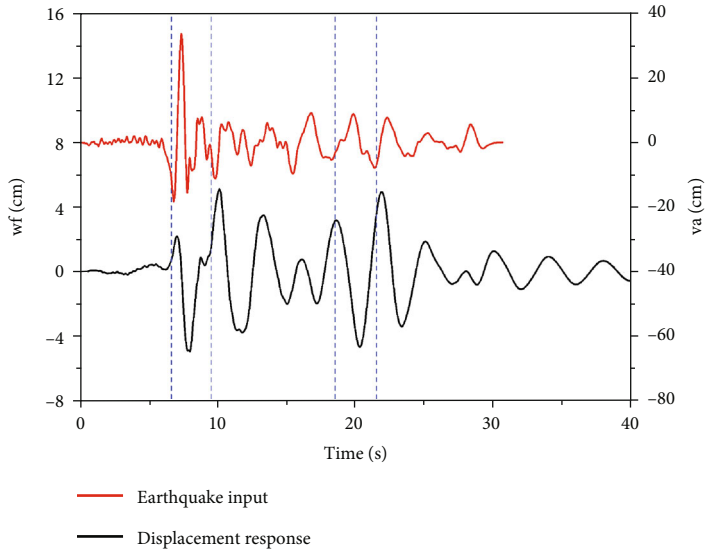

(a) Longitudinal direction with time

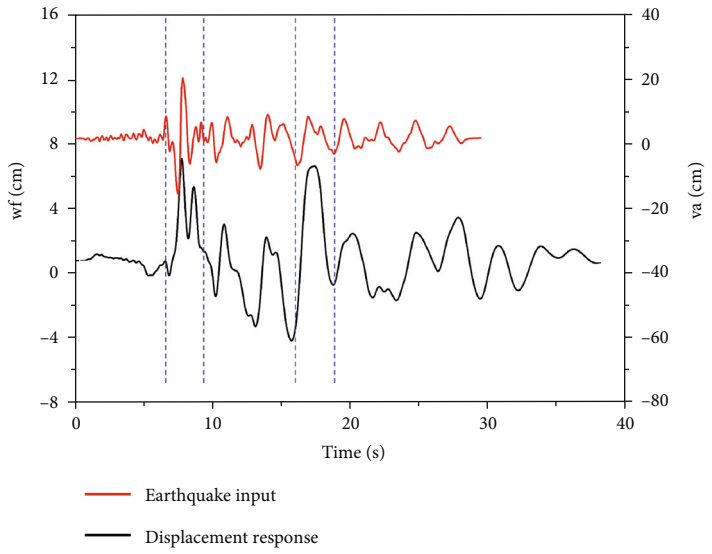

(b) Transverse direction with time

Figure 3: Continued.

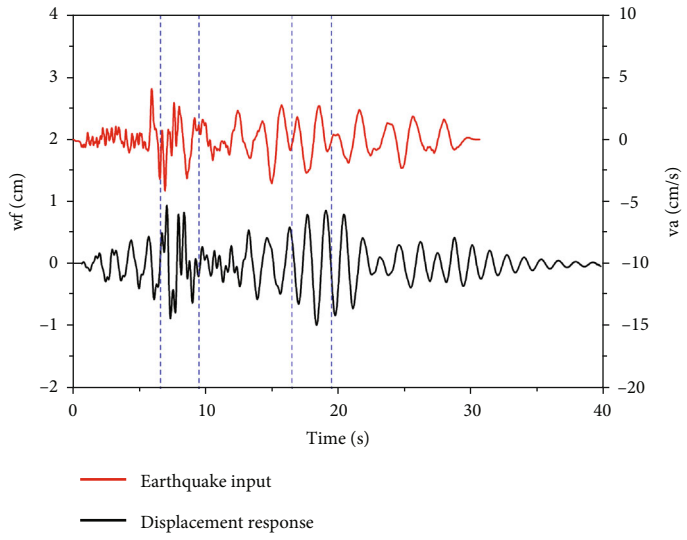

(c) Vertical direction with time

Figure 3: Displacement of the top of the arch during near-fault ground motion with time.

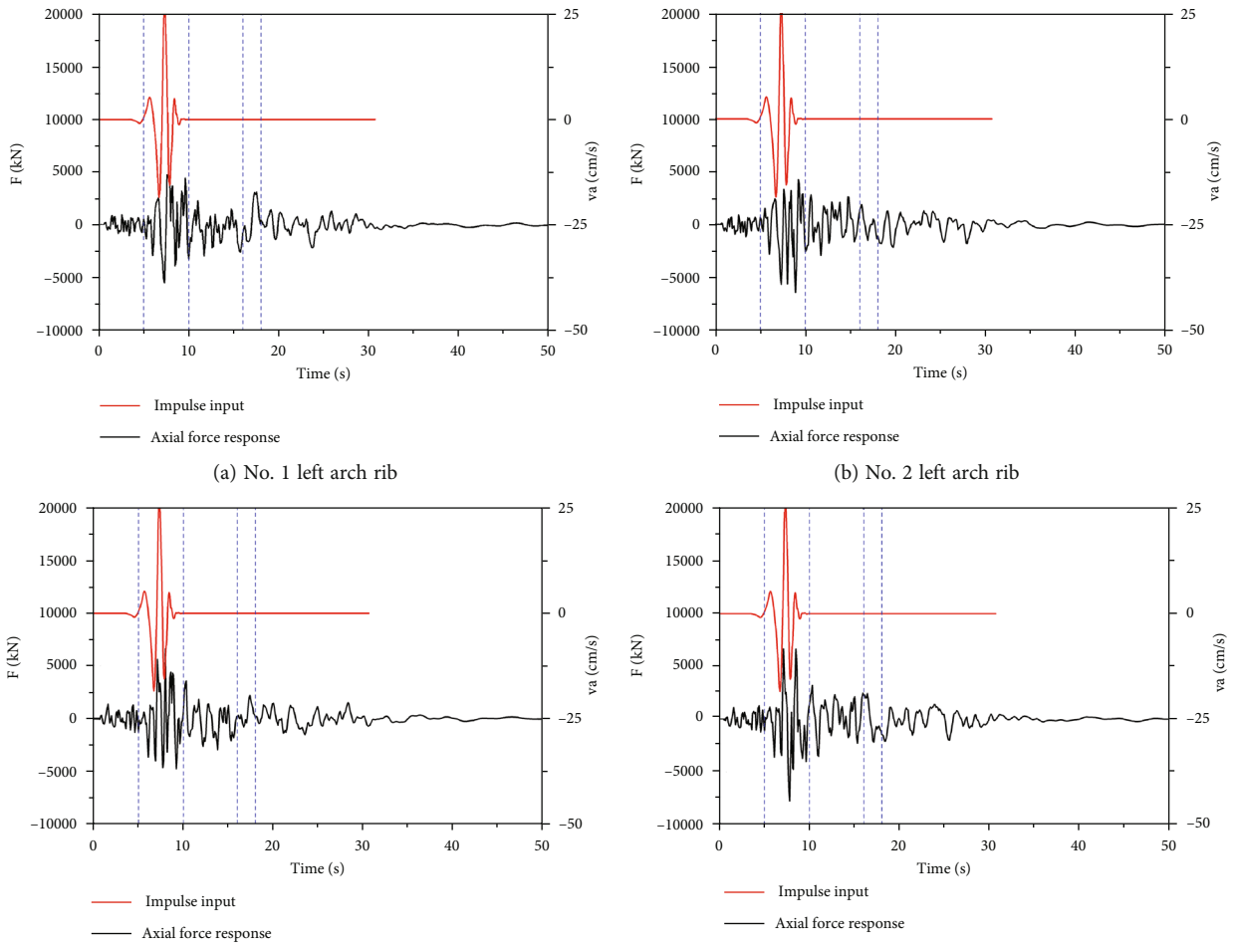

(a) No. 1 left arch rib

(b) No. 2 left arch rib

(c) No 1. right arch rib

(d) No. 2 right arch rib

Figure 4: Axial force response of support of the arch with time.

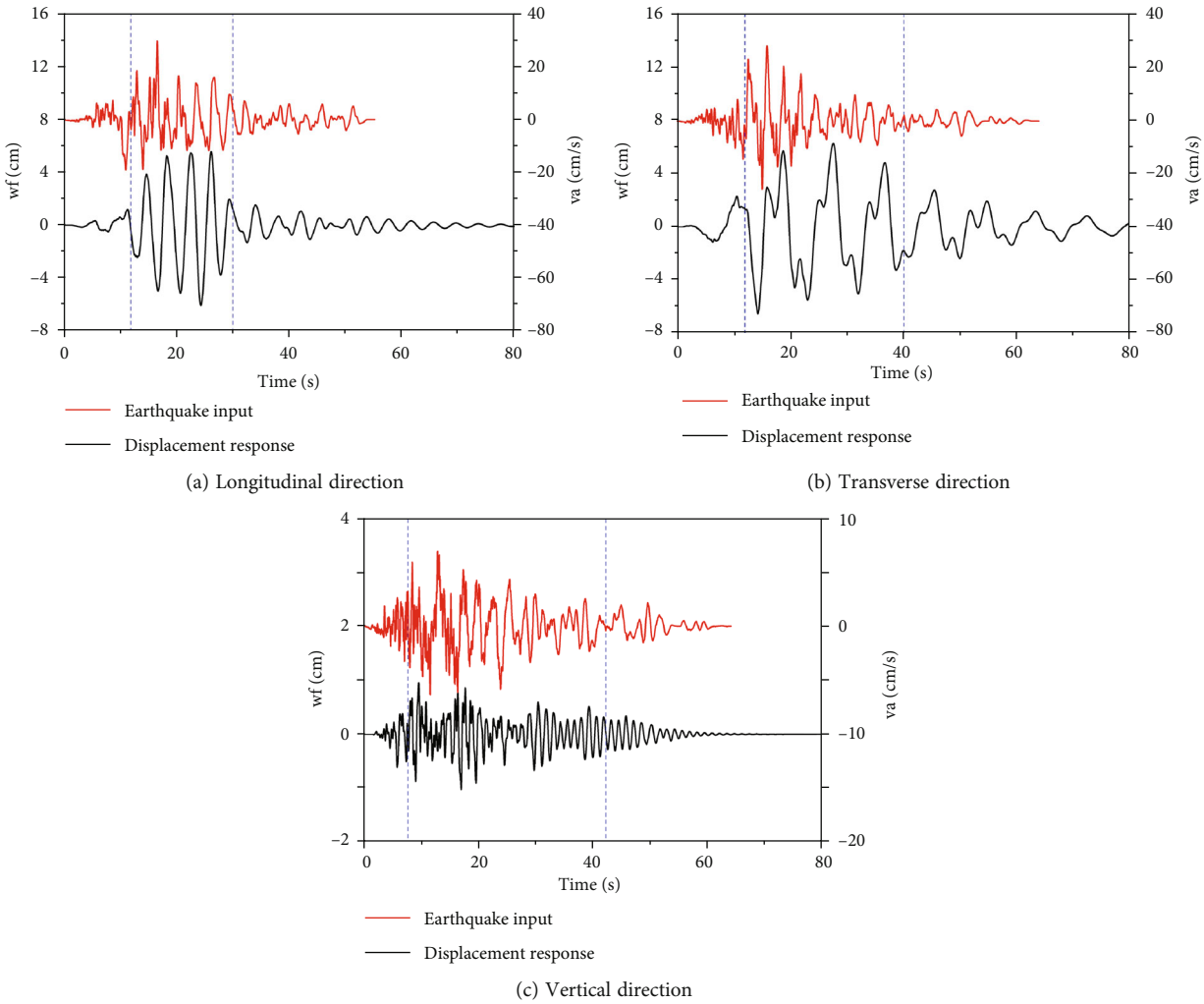

Figure 5: Displacement at the top of the arch during non-near-fault ground motion with time.

for the nonlinear analysis. The input excitation and the structural response with time at the arch support, top of the arch, and other locations on the bridge are shown in Figures 3 and 4.

A comparison and analysis of the displacement of key areas of the bridge with the corresponding input excitation values showed that the peak displacements do not occur at the time of the highest seismic input with a significant time lag of an accumulated time of about 10 s. For the axial force response, the time that the peak of the axial force appears is basically the same as the seismic excitation pulse.

This shows that for such large-span arch bridges with concrete-filled steel tubes, the high-velocity pulse from a near-fault earthquake is easy to produce a high axial force at the support of the arch which can cause damage to the arch support. The displacement of the arch rib is greatly affected by the total seismic energy and peaks during the attenuation of the seismic excitation due to the accumulated total energy absorbed by the structure. The contribution of a high-velocity pulse to the displacement is significantly related to the total energy of the pulse.

The similarities and differences between the near-fault and non-near-fault ground motions were compared in terms of the deformation mechanism and seismic damage to the bridge structure. The first group of inputted ground motions of the non-near-fault earthquakes has a similar intensity as the near-fault earthquakes. Figures 5 and 6 show the displacement and internal forces in the key areas through the seismic response analysis.

The results show that the non-near-fault ground motions cause large displacement of the bridge, which is even larger than that of the near-fault ground motions with the same peak ground acceleration (PGA). The seismic motion continues to transfer seismic energy into the bridge structure which causes the long duration of high intensity.

The seismic motion causes a larger displacement of the structure. The internal force of the support of the arch caused by the non-near-fault ground motions is not as high as that of the near-fault ground motions with the same PGA. The internal force at the arch support caused by non-near-fault ground motions continues to fluctuate within a certain range. The arch base produces large internal forces in a short

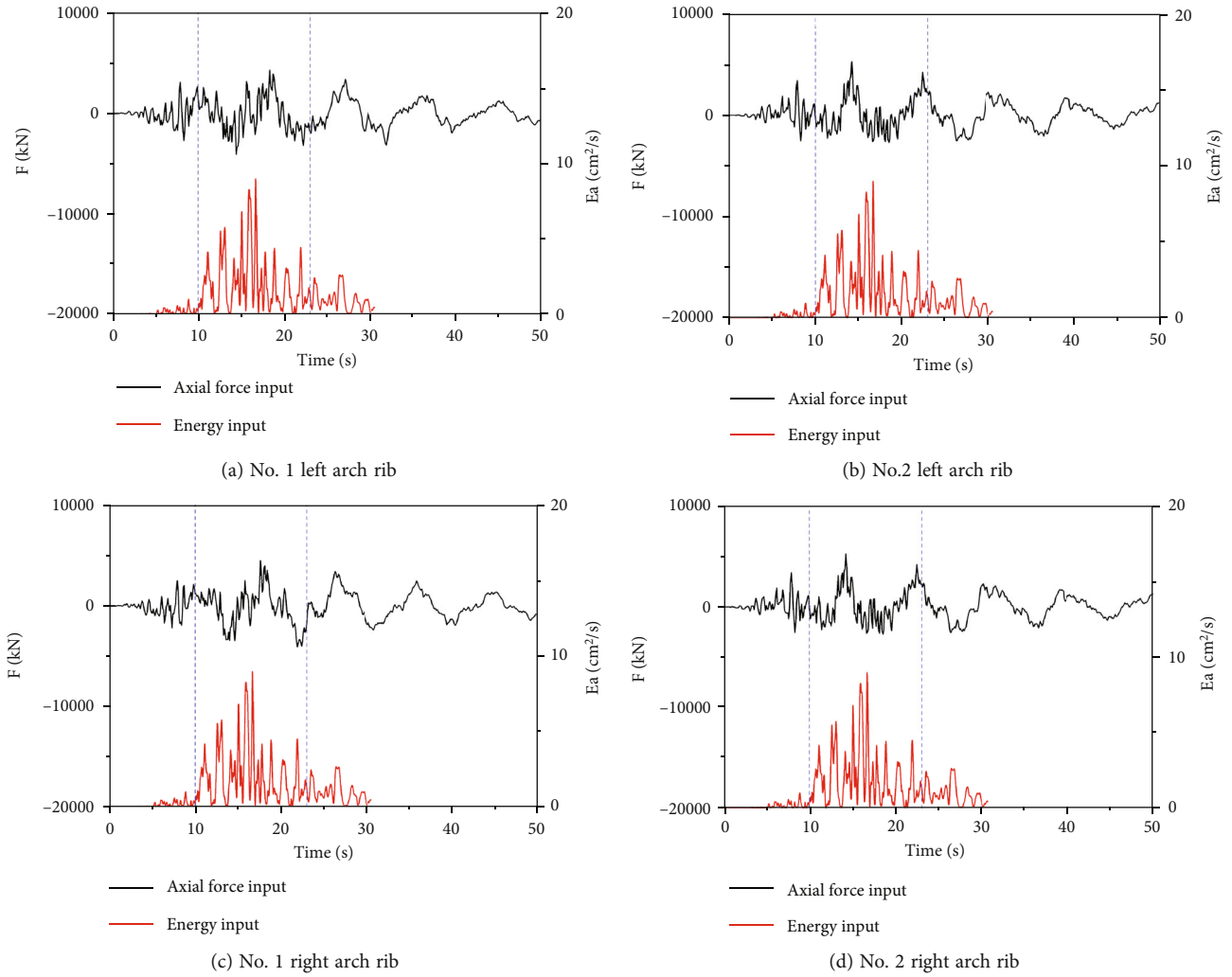

Figure 6: Axial force at the arch support during non-near-fault ground motion.

Table 4: Damage index range of bridge structure under different damage degrees.

Damage degree	Damage index range
Basic intact	0.00~0.20
Slightly damage	0.20~0.30
Moderate damage	0.30~0.50
Serious damage	0.50~0.70
Collapse	0.70~1.00

Table 5: Damage index of bridge components under near-fault ground motion.

Construct	Deformation	Energy	Weighted sum
Arch ribs	0.090	0.154	0.111
Wind brace	0.023	0.007	0.024
Suspension rods	0.017	0.177	0.041
Transverse beams	0.033	0.002	0.033
Longitudinal beams	0.022	0.001	0.022
Arch	0.034	0.071	0.044
Overall structure		0.103	

period of time due to the high pulses due to the near-fault ground motions, while the same amount of non-near-fault ground motions continue to transfer energy onto the bridge structure due to the absence of velocity pulses which produces larger displacement of the structure.

3.2. Damage Analysis of Whole Structure. In order to quantitatively compare the impact of the two types of ground motions on the tied-arch bridge as a whole, a double-damage criterion based on energy and displacement is used based on Xie et al. [40]. These criteria are used to assess damage based on the degree of component damage and energy absorption. It can well reflect the stress characteristics and failure modes of arch bridges with concrete-filled steel tubes. The degree of damage to the arch rib, suspension rods, and longitudinal and transverse beams is determined

Table 6: Damage index of bridge components under non-near-fault ground motion.

Construct	Deformation	Energy	Weighted sum
Arch ribs	0.092	0.107	0.107
Wind brace	0.025	0.006	0.026
Suspension rods	0.016	0.162	0.038
Transverse beams	0.067	0.002	0.067
Longitudinal beams	0.035	0.001	0.035
Arch	0.041	0.066	0.050
Overall structure		0.098	

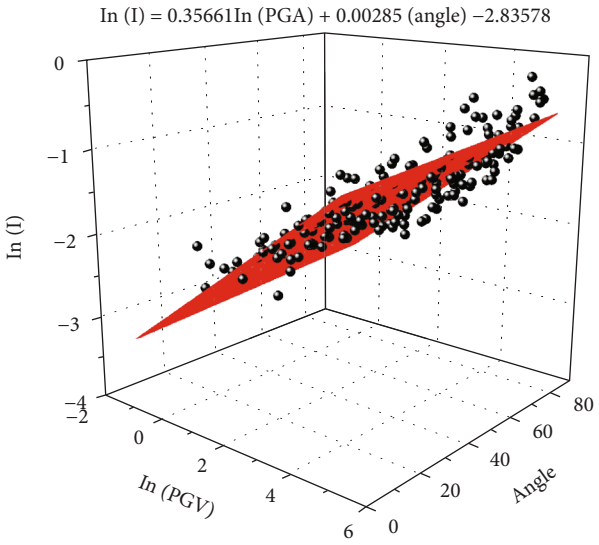

Figure 7: Three-dimensional relationship among velocity pulse, excitation angle, and bridge damage.

by using Equations (1) to (4) [40]:

$$\text{Arch rib}: I_{gl} = \frac{\lambda_m}{\lambda_u} + \alpha \frac{\int E_h dl}{\int (N_u \varepsilon_u + a M_u \varphi_u) dl}, \quad (1)$$

$$\text{Suspension rods}: I_{dg} = \frac{\varepsilon_m}{\varepsilon_u} + \alpha \frac{\int E_h dl}{\int N_u \varepsilon_u dl}, \quad (2)$$

$$\text{Longitudinal and transverse beams}: I_{hlzl} = \frac{\varepsilon_m}{\varepsilon_u} + \alpha \frac{\int E_h dl}{\int M_u \varphi_u dl}, \quad (3)$$

where I_{gl}, I_{dg}, and I_{hlzl} represent the damage index of the arch ribs, suspension rods, and longitudinal and transverse beams, respectively; λ_m and ε_m denote the maximum compressive bending stress and maximum strain of the arch rib, respectively, due to the seismic forces; λ_u, ε_u, ϕ_u, M_u, and N_u represent the limit values of the member's compressive bending coefficient, strain, curvature, bending moment, and axial force, respectively; E_h represents the energy accumulated in the section of the corresponding member due to the seismic forces; l is the length along the member; and α is a coefficient. As an example, an α of 0.139 is used based on [40].

The damage of each component during an earthquake is weighted according to the difference of its accumulated energy in calculating the total damage index.

$$\begin{cases} I = I_{gl} W_{gl} + I_{dg} W_{dg} + I_{hlzl} W_{hlzl}, \\ W_{gl} = \left(\dfrac{E_{gl}}{\sum E_{gl} + E_{dg} + E_{hlzl}} \right)_{gl}, \end{cases} \quad (4)$$

where I_{gl}, I_{dg}, and I_{hlzl} are the overall damage indexes of the arch ribs, suspension rods, and longitudinal and transverse beams, respectively; W_{gl}, W_{dg}, and W_{hlzl} are the overall damage indexes of the arch ribs, suspension rods, and longitudinal and transverse beams, respectively, and $\sum E_{gl}$, $\sum E_{dg}$, and $\sum E_{hlzl}$ are, respectively, the total energy accumulated in the arch rib, suspension rods, and longitudinal and transverse beams, during an earthquake. Based on the energy and displacement, these criteria comprehensively and quantify evaluate the damage to a bridge due to an earthquake. According to the provisions of [40] and recommendations in [38], the range of the bridge damage index for the different degrees of damage is defined in Table 4.

Combined with the above formulas, the damage of bridges was quantitatively calculated according to the seismic response of bridges under the action of near-fault ground motion and non-near-fault ground motion. The damage of each component is calculated, respectively, and listed in Tables 5 and 6.

Based on the analysis of the damage to the bridge due to the near-fault and non-near-fault earthquakes, it is found that most of the damage occurs at the arch ribs. The damage to the arch ribs is a significant part of the overall damage of the bridge, while the damage of the remaining parts is relatively limited with low energy absorption. The contribution to the overall damage to the bridge of these parts is very limited. The velocity pulses in the near-fault ground motions will increase the damage index based on the total accumulated energy, which in turn affects the overall state of damage.

The magnitude of an earthquake directly affects the stability and integrity of a structure. Similarly, the seismic data input for the Midas simulation program will significantly affect the response of the bridge structure especially for the near-fault ground motions which is highly directional. Changes in the inputted excitation angle of motion of the

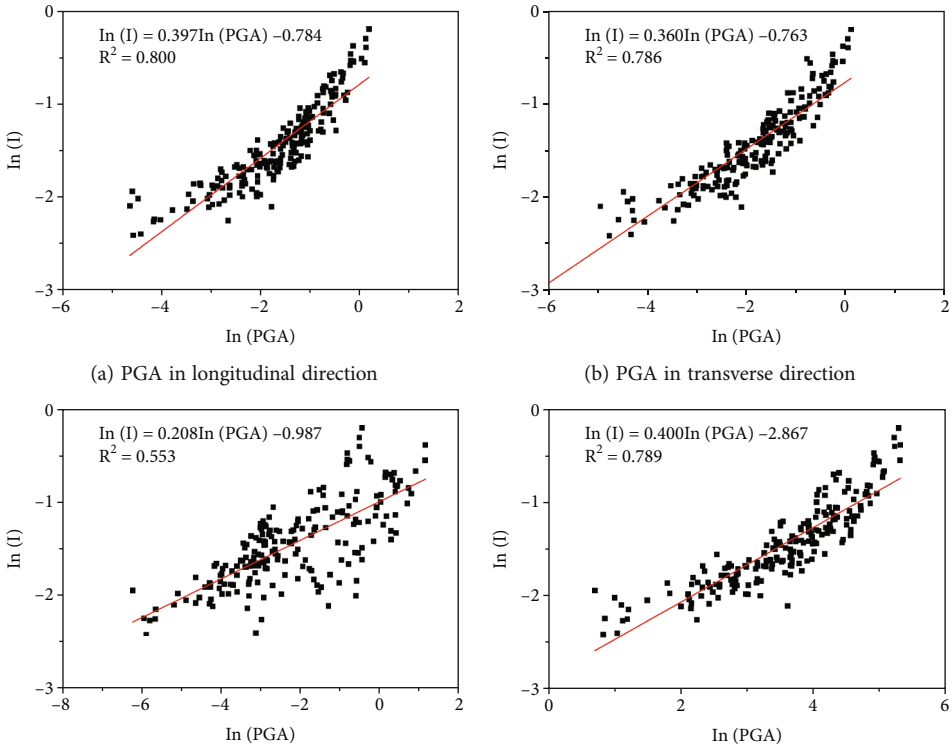

(a) PGA in longitudinal direction

(b) PGA in transverse direction

(c) PGA in vertical direction

(d) Intensity of velocity pulse

Figure 8: Plotted logarithmic relationship of intensity of near-fault ground motions vs. damage to the bridge.

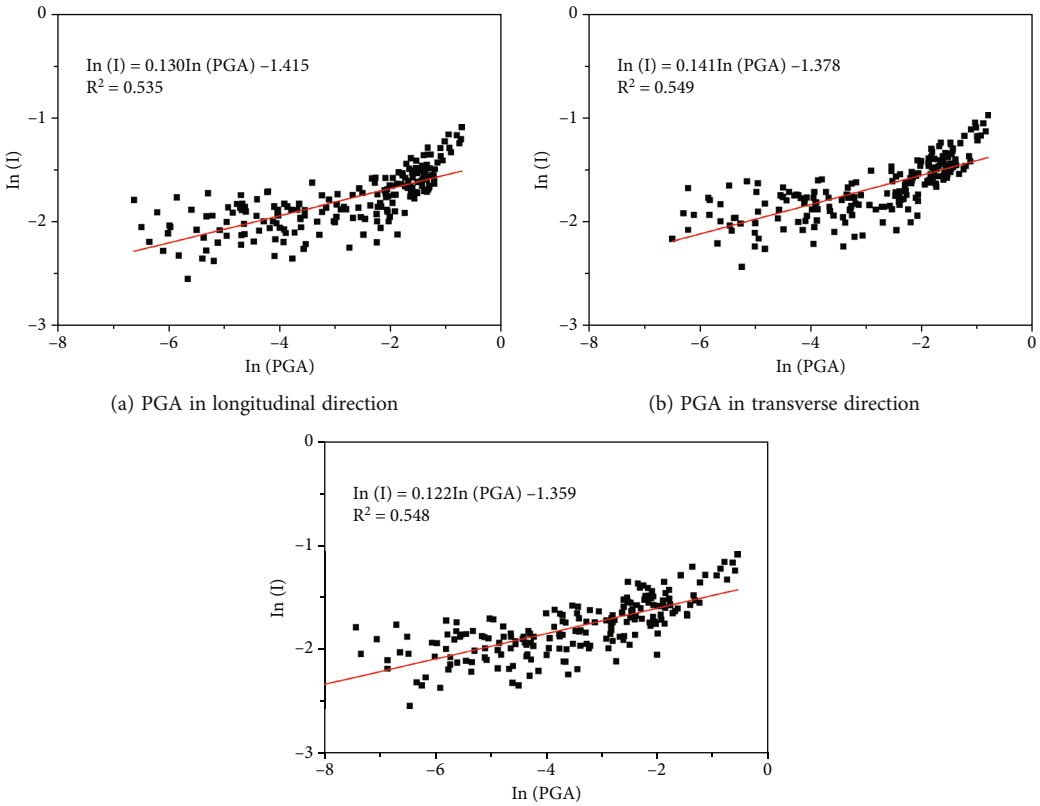

(a) PGA in longitudinal direction

(b) PGA in transverse direction

(c) PGA in vertical direction

Figure 9: Plotted logarithm relationship of intensity of non-near-fault ground motions vs. damage to the bridge.

Table 7: Damage probability of various failure states.

Type of earthquake	Direction	Earthquake intensity rating (g)	Amount of damage			Collapse
			Minor	Moderate	Severe	
Near fault	Longitudinal	E1 (0.090)	44.20%	27.45%	12.09%	6.10%
		E2 (0.150)	53.22%	35.48%	17.27%	9.34%
		E3 (0.195)	57.82%	39.90%	20.41%	11.44%
		E4 (0.255)	62.41%	44.55%	23.94%	13.91%
	Transverse	E1 (1.176)	49.08%	31.55%	14.54%	7.55%
		E2 (1.960)	57.31%	39.24%	19.79%	10.96%
		E3 (2.548)	61.44%	43.39%	22.89%	13.09%
		E4 (3.332)	65.54%	47.71%	26.31%	15.55%
	Vertical	E1 (0.063)	52.54%	31.51%	12.13%	5.25%
		E2 (0.105)	58.18%	36.74%	15.26%	6.97%
		E3 (0.137)	61.03%	39.54%	17.05%	8.01%
		E4 (0.179)	63.87%	42.46%	19.02%	9.18%
Non-near-fault	Longitudinal	E1 (0.090)	43.56%	23.68%	7.86%	3.04%
		E2 (0.150)	47.16%	26.58%	9.27%	3.72%
		E3 (0.195)	49.01%	28.13%	10.07%	4.12%
		E4 (0.255)	50.92%	29.76%	10.94%	4.55%
	Transverse	E1 (1.176)	44.20%	24.41%	8.34%	3.31%
		E2 (1.960)	48.06%	27.56%	9.93%	4.10%
		E3 (2.548)	50.05%	29.25%	10.83%	4.56%
		E4 (3.332)	52.09%	31.03%	11.81%	5.07%
	Vertical	E1 (0.063)	45.33%	25.30%	8.77%	3.52%
		E2 (0.105)	48.68%	28.07%	10.19%	4.22%
		E3 (0.137)	50.40%	29.54%	10.98%	4.63%
		E4 (0.179)	52.17%	31.09%	11.83%	5.07%

structure will result in a substantial difference in the degree of damage.

Prior to inputting the ground motion data into Midas, the excitation angle of the ground motion is randomly generated and the intensity of the excitation is increased. In order to isolate the damage of near-fault ground motions to the bridge structure, nonuniform excitation has not been considered here. The seismic data is grouped by matching the intensity of the excitation and the excitation angle for the analysis. A total of 200 analyses were carried out. However, due to limitations in space, only the pulse intensity, excitation angle, PGA, and other information of the near-fault ground motions are used for the seismic damage index as shown in Figures 7–9.

Results show the three-dimensional plot of the relationship among the intensity of the velocity pulse, pulse excitation, and damage of the bridge with near-fault ground motions. This indicated that the pulse intensity significantly affects the degree of damage to the bridge. The damage in the transverse direction is much greater than that in the longitudinal direction; however, the impact of the pulse excitation angle on the damage to the bridge is not as significant as the pulse intensity. In order to better quantitatively determine the differences in damage between near-fault and non-near-fault ground motions, the damage probability of various failure states for four seismic intensity levels is listed in Table 7.

Results show the probability that the damage caused by near-fault earthquakes is higher than that for the non-near-fault earthquakes of the same level of intensity. This difference is more significant when there is severe damage and collapse of the structure. The probability of serious damage caused by near-fault earthquakes is 1.81 times that of non-near-fault earthquakes. This ratio is increased to 2.32 in damage that involves collapse of the bridge structure and 1.17 and 1.36 times that of non-near-fault earthquakes with minor and moderate damage, respectively. Furthermore, the stratum characteristics significantly affect the safety of bridge structures. The reinforced soil can provide a stable geological environment that can support the bridge base and the whole structure [41]. And the fact that water seepage action and even temperature effect play a very important role, the normalized thermal conductivity and the reciprocal of the saturation are linearly related [42].

4. Conclusions

In this study, the damage caused by near-fault ground motions on large-span arch bridges with concrete-filled steel tubes was examined based on a case study. Various near-

fault and non-near-fault ground motions are taken into consideration when imposing load onto the bridge, including the analysis on the displacement, overall response, internal force changes, and damage probability of the bridge, which provided the guidance for practical engineering.

Near-fault ground motions will result in greater damages than non-near-fault ground motions of the same intensity for a long-span tied-arch bridge with concrete-filled steel tubes. The degree of damage is measured by an increase in the probability of damage, and this increase is more significant for a structure that suffers more severe damage and collapse. This indicates that the presence of high-velocity pulses in near-fault ground motion makes low seismic intensity earthquakes more destructive thereby causing more damage to the structure of the bridge.

Near-fault velocity pulses with higher intensity will cause more obvious damage to the structure of bridges. A smaller angle between the pulse propagation direction and the transverse direction of the bridge will result in damages. The bridge being studied here has a large span and is relatively wide. Therefore, it is more prone to damage when it is subjected to motion in the transverse direction.

Near-fault and non-near-fault ground motions of similar intensity are examined. The magnitude of the displacement caused by the top of the arch and at the 1/4 arch rib is basically the same, but there is a 23% difference in the internal force at the arch support. After using the double-damage criteria based on component damage and energy absorption, the overall difference in the damage index is 5%. The stiffness of the arch support with concrete-filled steel tubes is extremely high, and the impact of high-velocity pulses in near-fault ground motions is likely to produce a large internal force and, subsequently, cause more damage.

The high-velocity pulses in near-fault ground motions contain extremely high levels of energy, which increases the possibility of severe damage to bridges and may cause some of the bridge components to fail earlier than the entire bridge due to reasons such as the direction of the pulse, thereby affecting the overall performance of the bridge. In order to ensure the structural integrity of large-span tied-arch bridges with concrete-filled steel tubes after being impacted by near-fault ground motions, the impact of velocity pulse on the damage of the bridge should be fully considered in the bridge design.

Data Availability

The calculated data used to support the findings of this study are included within the article.

Conflicts of Interest

No conflict of interest exits in the submission of this manuscript.

Authors' Contributions

The manuscript is approved by all authors for publication.

Acknowledgments

The authors would like to acknowledge the financial support received from the Science and Technology Project of Henan Province under Grant No. 212102310939 and No. 212102310596.

References

[1] F. Huang, Y. Cui, R. Dong, J. Wei, and B. Chen, "Evaluation on ultimate load-carrying capacity of concrete-filled steel tubular arch structure with preload," *Advances in Structural Engineering*, vol. 22, no. 13, pp. 2755–2770, 2019.

[2] B. Chen, Z. Lai, X. Lai, A. H. Varma, and X. Yu, "Creep-prediction models for concrete-filled steel tube arch bridges," *Journal of Bridge Engineering*, vol. 22, no. 7, p. 04017027, 2017.

[3] B. Kumari, "Concrete filled steel tubular (CFST) columns in composite structures," *IOSR Journal of Electrical and Electronics Engineering (IOSR-JEEE)*, vol. 13, no. 1, pp. 11–18, 2018.

[4] B. Chen and T. Wang, "Overview of concrete filled steel tube arch bridges in China," *Practice Periodical on Structural Design and Construction*, vol. 14, no. 2, pp. 70–80, 2009.

[5] J. Zheng and J. Wang, "Concrete-filled steel tube arch bridges in China," *Engineering*, vol. 4, no. 1, pp. 143–155, 2018.

[6] N. Hu, G. L. Dai, B. Yan, and K. Liu, "Recent development of design and construction of medium and long span high- speed railway bridges in China," *Engineering Structures*, vol. 74, pp. 233–241, 2014.

[7] L. Zhang and Y. Xie, "Design optimization of steel tubewall thickness of concrete-filled steel tubular arch bridge," *International Journal of Robotics and Automation*, vol. 36, no. 10, 2021.

[8] J. Zheng, H. Du, T. Mu et al., "Innovations in design, construction, and management of Pingnan Third Bridge-the largest-span arch bridge in the world," *Structural Engineering International*, vol. 32, no. 2, pp. 1–8, 2022.

[9] K. Xie, H. Wang, X. Guo, and J. Zhou, "Study on the safety of the concrete pouring process for the main truss arch structure in a long-span concrete-filled steel tube arch bridge," *Mechanics of Advanced Materials and Structures*, vol. 28, no. 7, pp. 731–740, 2021.

[10] Z. Huang, "The prospect of constructing "southward passage" in Southwest China," *Journal of Chongqing Jiaotong University (natural science edition)*, vol. 38, no. 11, pp. 1–5, 2019, In Chinese.

[11] W. Hou, J. Yang, Z. Zhang, and X. Yuan, "Experimental study and application of manufactured sand self-compacting concrete in concrete-filled-steel-tube arch bridge: a case study," *Case Studies in Construction Materials*, vol. 15, article e00718, 2021.

[12] M. Yang, C. Cai, and Y. Chen, "Creep performance of concrete-filled steel tubular (CFST) columns and applications to a CFST arch bridge," *Steel and Composite Structures*, vol. 19, no. 1, pp. 111–129, 2015.

[13] J. Alvarez, A. Aparicio, J. Jara, and M. Jara, "Seismic assessment of a long-span arch bridge considering the variation in axial forces induced by earthquakes," *Engineering Structures*, vol. 34, pp. 69–80, 2012.

[14] C. Liu, Y. Wang, W. Wang, and X. Wu, "Seismic performance and collapse prevention of concrete-filled thin-walled steel

tubular arches," *Thin-Walled Structures*, vol. 80, pp. 91–102, 2014.

[15] E. Murat and D. R. Reginald, "Bridge seismic response as a function of the friction pendulum system (FPS) modeling assumptions," *Engineering Structures*, vol. 30, no. 11, pp. 3204–3212, 2008.

[16] C. Shao, J. W. W. Ju, G. Han, and Y. Qian, "Seismic applicability of a long-span railway concrete upper-deck arch bridge with CFST rigid skeleton rib," *Structural Engineering and Mechanics*, vol. 61, no. 5, pp. 645–655, 2017.

[17] Y. Huang, B. Briseghella, T. Zordan, Q. Wu, and B. Chen, "Shaking table tests for the evaluation of the seismic performance of an innovative lightweight bridge with CFST composite truss girder and lattice pier," *Engineering Structures*, vol. 75, pp. 73–86, 2014.

[18] L. Xin, X. Li, Z. Zhang, and L. Zhao, "Seismic behavior of long-span concrete-filled steel tubular arch bridge subjected to near-fault fling-step motions," *Engineering Structures*, vol. 180, pp. 148–159, 2019.

[19] K. Bi, H. Hao, and W. X. Ren, "Seismic response of a concrete filled steel tubular arch bridge to spatially varying ground motions including local site effect," *Advances in Structural Engineering*, vol. 16, no. 10, pp. 1799–1817, 2013.

[20] S. X. Zheng, X. H. Shi, H. Y. Jia, C. H. Zhao, H. L. Qu, and X. L. Shi, "Seismic response analysis of long-span and asymmetrical suspension bridges subjected to near-fault ground motion," *Engineering Failure Analysis*, vol. 115, article 104615, 2020.

[21] X. Chen, Y. Liu, B. Zhou, and D. Yang, "Seismic response analysis of intake tower structure under near-fault ground motions with forward-directivity and fling-step effects," *Soil Dynamics and Earthquake Engineering*, vol. 132, article 106098, 2020.

[22] F. Huang, C. Fu, Y. Zhuang, and Z. H. Xiong, "Experiment on seismic performance of concrete filled steel tubular arch-rib under multi-shaking-tables," *Thin-Walled Structures*, vol. 116, pp. 212–224, 2017.

[23] S. Li, F. Zhang, J. Q. Wang, M. S. Alam, and J. Zhang, "Effects of near-fault motions and artificial pulse-type ground motions on super-span cable-stayed bridge systems," *Journal of Bridge Engineering*, vol. 22, no. 3, p. 04016128, 2017.

[24] Q. Wu, M. Yoshimura, K. Takahashi, S. Nakamura, and T. Nakamura, "Nonlinear seismic properties of the Second Saikai Bridge: a concrete filled tubular (CFT) arch bridge," *Engineering Structures*, vol. 28, no. 2, pp. 163–182, 2006.

[25] X. Li, D. Zhang, W. Yan, W. Xie, and M. D. Pandey, "Effects of model updating on the estimation of stochastic seismic response of a concrete-filled steel tubular arch bridge," *Structure and Infrastructure Engineering*, vol. 10, no. 12, pp. 1620–1637, 2014.

[26] G. P. Mavroeidis, G. Dong, and A. S. Papageorgiou, "Near-fault ground motions, and the response of elastic and inelastic single- degree-of-freedom (SDOF) systems," *Earthquake Engineering & Structural Dynamics*, vol. 33, no. 9, pp. 1023–1049, 2004.

[27] S. F. Ghahari, H. Jahankhah, and M. A. Ghannad, "Study on elastic response of structures to near-fault ground motions through record decomposition," *Soil Dynamics and Earthquake Engineering*, vol. 30, no. 7, pp. 536–546, 2010.

[28] F. Xing, X. F. Li, and X. Li, "Action effect of near fault earthquake on bird type concrete filled steel tube arch bridge," *Engineering seismic and reinforcement*, vol. 38, no. 4, pp. 42–47, 2016, In Chinese.

[29] A. Moustafa and I. Takewaki, "Deterministic and probabilistic representation of near-field pulse-like ground motion," *Soil Dynamics and Earthquake Engineering*, vol. 30, no. 5, pp. 412–422, 2010.

[30] B. Bai, R. Zhou, G. Cai, W. Hu, and G. Yang, "Coupled thermo-hydro-mechanical mechanism in view of the soil particle rearrangement of granular thermodynamics," *Computers and Geotechnics*, vol. 137, no. 8, article 104272, 2021.

[31] B. Yuan, Z. Li, Z. Zhao, H. Ni, Z. Su, and Z. Li, "Experimental study of displacement field of layered soils surrounding laterally loaded pile based on transparent soil," *Journal of Soils and Sediments*, vol. 21, no. 9, pp. 3072–3083, 2021.

[32] X. Li, L. He, Q. Li, and Y. Pan, "Analysis of the influence of pulse ground motion on seismic performance of CFST arch bridge," *Journal of Southwest Jiaotong University*, vol. 54, no. 4, pp. 731–740, 2019, In Chinese.

[33] W. Liao, C. Loh, S. Wan, W. Y. Jean, and J. Chai, "Dynamic responses of bridges subjected to near-fault ground motions," *Journal of the Chinese Institute of Engineers*, vol. 23, no. 4, pp. 455–464, 2000.

[34] Z. Liu, X. Han, and Z. Zhang, "Seismic damage analysis of flying swallow type concrete filled steel tube arch bridge based on traveling wave effect," *Journal of Sichuan University (Engineering Science Edition)*, vol. 47, no. 6, pp. 54–60, 2015, In Chinese.

[35] Z. Liu, Z. Zhang, and Y. Wang, "Seismic vulnerability analysis of concrete filled steel tubular arch bridge based on near fault effect," *Journal of Wuhan University of Technology (transportation science and engineering edition)*, vol. 40, no. 5, pp. 815–819, 2016, In Chinese.

[36] M. Keita, T. Kazuo, and N. Shozo, "Validation of the vibration model for a CFT arch bridge (New Saikai Bridge)," *Journal of Psychosomatic Research*, vol. 58, no. 1, pp. 103–110, 2009.

[37] S. K. Shahi and J. W. Baker, "An efficient algorithm to identify strong-velocity pulses in multicomponent ground motions," *Bulletin of the Seismological Society of America*, vol. 104, no. 5, pp. 2456–2466, 2014.

[38] C. Communications and highway planning and Design Institute Co., Ltd., *General Code for Design of Highway Bridges and Culverts*, People's Communications Press Co., Ltd., In Chinese, 2015.

[39] China seismological bureau, "China seismic intensity scale," 2020, In Chinese.

[40] K. Xie, W. Lv, L. Qin, and F. Meng, "Seismic damage assessment of concrete filled steel tubular arch bridge," *Chinese Journal of highway*, vol. 25, no. 2, pp. 53–59, 2012, In Chinese.

[41] B. Yuan, Z. Li, Y. Chen et al., "Mechanical and microstructural properties of recycling granite residual soil reinforced with glass fiber and liquid-modified polyvinyl alcohol polymer," *Chemosphere*, vol. 286, Part 1, article 131652, 2022.

[42] B. Bai, Y. Wang, D. Rao, and F. Bai, "The effective thermal conductivity of unsaturated porous media deduced by pore-scale SPH simulation," *Frontiers in Earth Science*, vol. 10, article 943853, 2022.